View metadata, citation and similar papers at core.ac.uk
brought to you by CORE
provided by RERO DOC Digital Library

Synchrotron x-ray μ-tomography to model the thermal radiative properties of an opaque ceramic coating at $T = 1000$ K

B. Rousseau,[a] H. Gomart, and D. Zanghi
Conditions Extrêmes et Matériaux: Haute Température et Irradiation, 45071 Orléans, France

D. Bernard
Institut de Chimie de la Matière Condensée de Bordeaux, 33608 Pessac, France

M. Stampanoni
Swiss Light Source (SLS), Paul Sherrer Institute (PSI), Villigen, Switzerland; and Institute for Biomedical Engineering, University and Eidgenössische Technische Hochschule (ETH) Zürich, Zürich, Switzerland

(Received 8 October 2009; accepted 10 May 2010)

Synchrotron x-ray μ-tomography has been used to reconstruct the three-dimensional view of a rough surface extracted from a heterogeneous ceramic coating composed of $Pr_2NiO_{4+\delta}$. Radiographs with a resolution of 0.7 μm have been recorded at $T = 300$, 600, and 900 K. The analysis of surface geometry makes use of the geometrical optic approximation up to $T = 900$ K possible. Subsequently, a large number of rays (10^5) are impinged onto the numerical surface, as revealed by x-ray tomography, to reproduce the normal emissivity of the coating. This normal emissivity was obtained beforehand by infrared emittance spectroscopy at $T = 1000$ K. Comparison of the two approaches suggests that the optical contribution of the coating micropores can be integrated into the ray tracing code. The effective medium approximation is used for this purpose. Finally, the applicability of this hybrid approach is discussed.

I. INTRODUCTION

The texture of heterogeneous materials mainly influences their thermal radiative properties. The term texture is used to describe the spatial arrangement of the scatterers (pores, grains, cracks, and grain boundaries) within a host matrix and their respective size distributions. Depending on attenuation of the incident wave within a given material, two classes of optical system can be defined. The first system deals with materials for which the optical properties are governed by volumetric scattering mechanisms in the mid-infrared range. The absorption mechanisms of the host matrix allow for the propagation of light at distances generally greater than the thickness of the illuminated material. These optical systems are considered optically thin. The second system involves compounds for which an incident beam is attenuated over a length less than its thickness. In this case, the materials are defined as opaque or optically thick.

In particular, for opaque materials, their optical behavior is governed by their geometrical surface. Several studies have already attempted to connect the radiative properties of rough materials with the statistical parameters describing their surface roughness. Thus, it has been shown that treatments of the interaction of light with a given rough surface require one to deal with root mean square (rms) roughness and correlation length.[1] Knowledge of both the rms roughness and correlation length values allow for selection of the correct physical approximation, simplifying the mathematical treatment of the electromagnetic waves with matter. These geometrical parameters are also used for predicting the thermal radiative properties of opaque media through the appropriate mathematical formulas.[2] Therefore, these considerations show, for a given temperature, that knowledge of the topological description of a rough surface is crucial for accurate prediction of its radiative properties. Usually, the characteristic length scale of the surface dictates that its two-dimensional (2D) quantification is performed by using devices such as an atomic force microscope, an optical and/or mechanical profilometer, and a stereoscopic reconstruction based on a combination of images acquired by scanning electron microscopy (SEM). However, these devices are not often equipped with high-temperature furnaces to reach the prescribed temperature. It is worth noting that an SEM can offer this possibility, but the acquisition of images with good qualities at high temperature ($T \sim 1000$ K) requires performing the investigation only on a small area ($\sim 140 \times 140$ μm^2). This difficulty is due to thermal instabilities of the SEM system, which may make accurate numerical simulation of the radiative properties difficult. Indeed, modeling the radiative properties of a rough surface ($\sim 1000 \times 1000$ μm^2)

[a]Address all correspondence to this author.
e-mail: benoit.rousseau@cnrs-orleans.fr
DOI: 10.1557/JMR.2010.0244

Downloaded from https://www.cambridge.org/core. University of Basel, on 10 Oct 2017 at 14:17:03, subject to the Cambridge Core terms of use, available at https://www.cambridge.org/core/terms. https://doi.org/10.1557/JMR.2010.0244

requires performing calculations from a representative elementary surface, allowing for results similar to those that can be experimentally determined.[3] Three-dimensional (3D) nondestructive investigation techniques, such as x-ray μ-tomography (SRXTM), appear to be good candidates for extracting geometrical surface information, especially because they can be easily coupled with furnaces to attain high temperatures (∼1300 K).[3] We note that in other fields, SRXTM has already been used to characterize room temperature surface morphological properties, including measurement of fracture geometry in the geosciences,[4,5] fretting fracture in tribology,[6] and coral surface area in coral reef science.[7] Present day resolutions available with this technique can reach values on the order of 0.3 μm due to the use of specialized equipment.[8] This equipment allows a new type of investigation of the 3D texture of refractory ceramics with submicron pores.

This work describes characterization of the topology of the surface of a praseodymium nickelate ($Pr_2NiO_{4+\delta}$) coating at temperatures between 300 and 900 K, using SRXTM. The dependence of the statistical parameters[2,9] on the rough surface (rms roughness and correlation length) versus temperature is also reported. These data are then used to model the normal spectral emissivity of the coating at $T = 1000$ K. The modeling is based on a hybrid numerical code, developed recently,[10,11] that takes into account the textural features of a coating with different length scales. The term "hybrid" refers to the ability to take into account two well-distinguished length scales of heterogeneity, l_H and l_h, with $l_H \gg l_h$. The optical response of the greatest heterogeneity can be treated with the geometrical optic approximation ($l_H \gg \lambda$), whereas the optical response of the smallest heterogeneity can be reproduced with the effective approximation medium ($l_H \ll \lambda$). Finally, the results are compared with those obtained by room temperature characterization of the surface with a mechanical profilometer.

II. HIGH TEMPERATURE SURFACE CHARACTERIZATION

A. Synchrotron SRXTM experiment

A parallelepipedic sample of height 1000 μm and area 385 × 385 μm² was studied. The sample consisted of a rough coating of $Pr_2NiO_{4+\delta}$ covering an aluminosilicate block. The rough deposit had been obtained beforehand from a spray pyrolysis process.[12] The thickness of the coating was around 20 μm. An environmental scanning electron microscopy (ESEM) image acquired at $T = 300$ K (Fig. 1) indicates that the coating is composed of nonconnected grains. The sample was characterized by SRXTM from the tomographic microscopy and coherent adiology experiments (TOMCAT) beamline at the Paul Shererer Institute (PSI) for Swiss Light Source (SLS).[13] A gas blower furnace, loaned by the European Synchrotron Radiation Facility (ESRF),[8,14] was used to heat the sample to $T = 900$ K. During the experiment, the gas blower was monitored outside of the experimental hutch. To avoid undesirable thermal effects from the hot air flux coming from the furnace, both the Ce-doped $Y_3Al_5O_{12}$ single crystal scintillator and the rotating stage were protected with thin aluminum sheets. In addition, a cold air flux was permanently swept onto the surface of the scintillator to maintain a suitable operating temperature (to keep its efficiency constant). More details concerning the SRXTM setup can be found in Ref. 13. The rotation stage was moved 60 mm with respect to its normal room temperature configuration along the x-ray beam direction to minimize undesirable thermal effects on the electronic part of the detection chain. The scintillator was coupled to a visible light charge-coupled device (PCO2000, Kelheim, Germany) equipped with a 2048 × 2048 interline chip with a 7.4 × 7.4 μm² pitch. To homogenize the temperature within the volume of the heated specimen, a molybdenum thermal shield was positioned around the homemade sample holder, which was composed of an alumina rod that was fixed to the rotating sample holder. A thermal shield prevents thermal gradients within the sample's volume that are likely to generate inhomogeneous evolution of the sample's texture. A 10× objective was used, giving a field of view of 1.51 × 1.51 mm² with a pixel size of 0.7 μm. For the tomographic data acquisition, 721 projections of 1022 × 318 pixels were acquired per 180° with a 1 s exposure time per projection at photon energy of 35 keV. The 35 keV photons were sufficiently hard to allow reasonable x-ray transmission through the $Pr_2NiO_{4+\delta}$ coating with a diagonal length of 545 μm (linear attenuation coefficient, μ, equals ∼49.4 cm^{-1}, according to Ref. 15). This setup produced high-quality raw projection images for the temperature range (i.e., 300–900 K). Specific algorithms developed at the Institut de Chimie de la Matière

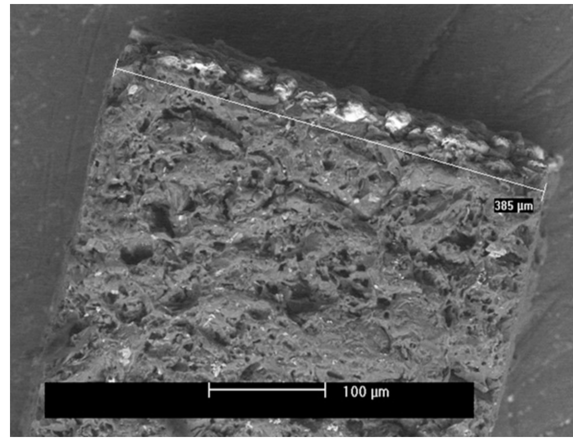

FIG. 1. ESEM image of the scanned sample (200×).

Downloaded from https://www.cambridge.org/core. University of Basel Library, on 11 Jul 2017 at 14:25:10, subject to the Cambridge Core terms of use, available at https://www.cambridge.org/core/terms. https://doi.org/10.1557/JMR.2010.0244

Condensée de Bordeaux (ICMCB), Bordeaux, France were applied to remove different artifacts (hot spots and rings) and the corrected projections were input into a filtered back-projection algorithm to reconstruct the distribution of the attenuation coefficient within the volume of the sample. Two filters (3D median and 3D anisotropic diffusion) were applied to the 32 bit reconstructed slices to ameliorate somewhat the effect of sample movements induced by the thermal load and of phase contrast induced by the large distance between the sample and the detector. The volumes considered for further postprocessing were cropped to 360 × 360 × 80 voxels and transformed into 8 bits (Fig. 2). These latter cropped samples contained all of the voxels physically corresponding to the rough $Pr_2NiO_{4+\delta}$ coatings.

The next operation consisted of measuring the air/$Pr_2NiO_{4+\delta}$ surfaces, which can be experimentally performed with the tip of a mechanical profilometer. To extract 2D images of the sample surface from the three volumes, the surface voxels were projected onto a plane parallel to the basal plane of the aluminosilicate substrate and touching the surface at at least one point. Note that the three volumes correspond to the same sample for $T = 300$ K, $T = 500$ K, and $T = 900$ K. For each voxel (coded in gray levels $0 \rightarrow 255$) with an intensity higher than 95, the distance to this plane was calculated and reported in a regular array with a step of 0.7 μm. The resulting images of 320 × 320 pixels were filtered with a minimum filter to close the smallest holes (Fig. 3). Comparing the three images, differences of a few pixels were found, leading to the conclusion, after considering the complexity of the processing necessary to obtain them, the rough surface is stable in this range of temperature. To gain further insight on the spatial organization of the surfaces, we used statistical tools to describe it.

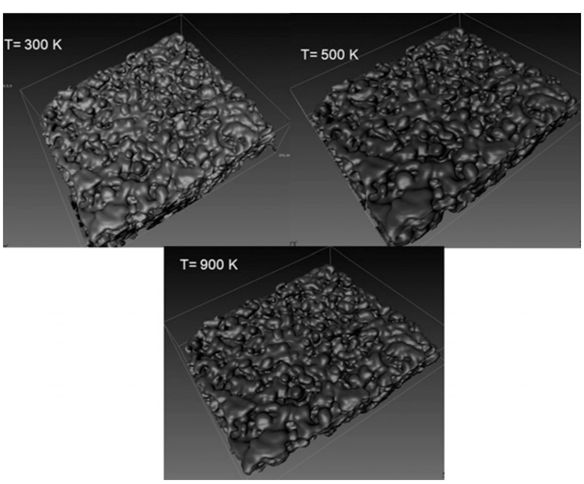

FIG. 2. Visualization of the rough surface at $T = 300$ K, $T = 500$ K, and $T = 900$ K.

B. Statistical description of the rough surfaces

For a given temperature, a square area of 225 × 225 μm^2 was selected and was stored in a N^2 array with $N = 320$. For the array, the size, δ, along both the x axis and y axis, was $\delta_x = \delta_y = 0.7$ μm. It provided N^2 values of height data, $z_{i,j}$, at the pixel (i, j) that were afterwards used to obtain the following statistical function of zero-order:

$$\omega_{\mathrm{rms}}^2 = \frac{1}{N^2} \sum_{i=0}^{N-1} \sum_{j=0}^{N-1} z_{i,j}^2 \quad , \tag{1}$$

where ω_{rms}^2 is the square of the quadratic mean, which is a measure of the magnitude of $z_{i,j}$. Its root is known as the rms. Another function of second-order is the autocorrelation function, $R(u, \upsilon)$:

$$R(u, \upsilon) = \frac{1}{(N-u)(N-\upsilon)} \sum_{i=0}^{N-1-u} \sum_{j=0}^{N-1-\upsilon} z_{j+\upsilon,i+u} z_{j,i} \quad , \tag{2}$$

where (u, υ) are the coordinates of the displacement vector for the case of an isotropic surface. The characteristic shape of this function indicates the kind of surface that is being investigated: Gaussian, exponential, or self-affine. Interesting lengths extracted from this function are the correlation lengths τ_u and τ_υ defined by:

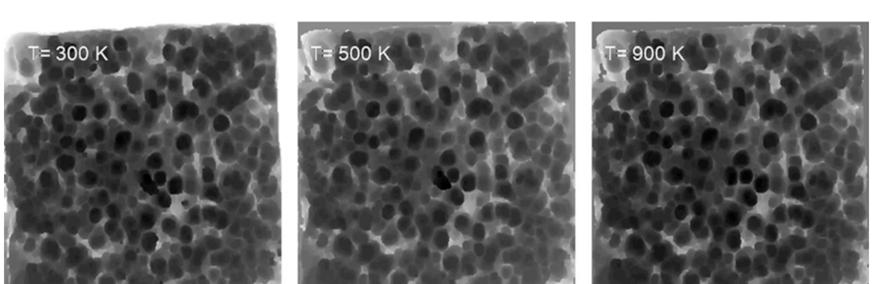

FIG. 3. 2D representation of the sample surface at the three considered temperatures. For these three images, the black color corresponds to distance zero and the white color corresponds to distance 255, which are attributed to each respective pixel. The unit size of a voxel is 0.7 μm so that the largest holes have a depth of 180 μm.

Downloaded from https://www.cambridge.org/core. University of Basel Library, on 11 Jul 2017 at 21:54:17, subject to the Cambridge Core terms of use, available at https://www.cambridge.org/core/terms. https://doi.org/10.1557/JMR.2010.0244

$$R(\tau_u, \tau_\upsilon) = R(0,0)1/e \quad , \tag{3}$$

where e is Euler's number and where $(u, \upsilon) = (0, 0)$. Equation (3) means that τ_u and τ_υ are the displacement lengths at which the autocorrelation function drops to $1/e$ of its peak value at $(u, \upsilon) = (0, 0)$. For an isotropic rough surface, $\tau_u = \tau_\upsilon = \tau$. In this case, the correlation length τ is also defined as the length for which two points are no longer correlated. This parameter controls the speed of the height changes along a given distance. For the three temperatures, the surface can be described as nearly Gaussian and isotropic. Table I lists the values of ω_{rms} and τ for the three temperatures used in this work. Note that the temperature has no influence on the values of ω_{rms} and τ, which indicates that the studied surface remains stable during the entire heating process.

Moreover, both of these values are useful in modeling the radiative behavior of the surface.[1,16] Rigorous treatment of light matter interaction requires solving the Maxwell equations. However, for a complex surface, finding the solutions to these equations can be tricky and computationally intensive. To counteract this difficulty, approximation schemes can be used, such as the Kirchhoff approximation and the small perturbation theory, whose regimes of validity can be questionable. It is also possible to use the geometrical optic approximation that can predict accurate radiative properties not only for opaque media,[2,17] but also for semitransparent media.[18] This approximation assumes that

(i) interference effects and diffraction can be neglected,

(ii) the tangent plane approximation is valid at the local impact point, and

(iii) an impinging ray is specularly reflected, and its energy is calculated from Fresnel's coefficients.

Moreover, this technique requires increasingly less computational effort due to increasing computer power. Tang and coworkers[1] have established a validity domain for 2D, rough, perfectly conducting surfaces for which the surface statistical parameters have to obey to

$$\omega_{rms} \cos(\theta)/\lambda > 0.17 \quad ,$$

and

$$\omega_{rms}/\tau < 0.4 \quad .$$

TABLE I. Statistical parameters used for the characterization of the SRXTM image and obtained by mechanical profilometry (see Ref. 10).

Li	SRXTM	SRXTM	SRXTM	MP (11)
	$T = 300$ K	$T = 500$ K	$T = 900$ K	$T = 300$ K
ω_{rms} (μm)	5.5	5.7	5.6	7.7
τ (μm)	8.4	8.7	8.3	24
α	0.93	0.93	0.95	0.45

For MP, the data was recorded with an Altisurf 500 device (Altimet, Thonon-Les-Bains, France) equipped with a stylus of 1 μm.

Here, λ is the incident wavelength and θ is the incident angle. Because the objective of this work is to model radiative properties for the spectral range (2–25 μm), it is obvious, according to the values of ω_{rms} and τ at $T = 900$ K, that the geometrical optics approximation is valid. In the latter part of this study, Monte Carlo ray tracing, developed to model the radiative behavior of random media, will be used.[2,10,18]

III. RESULTS AND DISCUSSION

In this work, a Monte Carlo ray tracing (MCRT) program for reproducing the spectral dependence (2–25 μm) of the thermal radiative properties (reflectivity, transmittivity, and emissivity) of heterogeneous materials over a large range of temperatures (300 to 1300 K) was applied.[18] Briefly, in the Monte Carlo method, a large number of rays impinge a sample and are traced numerically until they leave. The rays are able to move within the volume of the sample until they are absorbed by the solid phase. According to the optical properties of the solid phase on the local scale and to the texture of the sample, the propagation of the rays can be restricted to the surface and/or can be extended to the whole volume. At each interaction, the laws of geometrical optics are used to determine the behavior of a given ray at the local scale.

Kirchhoff's second law, involving knowledge of both the normal hemispherical spectral reflectivity $\hat{R}(\sigma, T)$ and the normal hemispherical spectral transmittivity, $\hat{T}(\sigma, T)$, is used to get the normal spectral emissivity, $E(\sigma, T)$. In these expressions, σ and T are the wave number (cm^{-1}) and the temperature (K), respectively, and $\sigma = 1/\lambda$. Due to its intrinsic optical properties, a $Pr_2NiO_{4+\delta}$ ceramic is considered opaque for a thickness higher than 2.5 μm. In the present case, the thickness of the ceramic is around 20 μm so that $\hat{T}(\sigma, T) \cong 0$. The normal spectral emissivity is thus expressed by

$$E(\sigma, T) = 1 - \hat{R}(\sigma, T) \quad . \tag{4}$$

Therefore, the MCRT architecture reproduced the experimental conditions that allowed the measurement of $\hat{R}(\sigma, T)$. A cylindrical beam ($\varnothing = 250$ μm) of N_{rays} rays, parallel and unpolarized was launched normally (along the z axis) toward the center of the reconstructed surfaces (see Fig. 2). Each ray carries an intensity I_0 equal to unity. The origins (x_{ray}, y_{ray}) of the rays were randomly distributed with a uniform weight inside the beam. Moreover, for each ray, $z_{ray} = a$, where a is a constant value. Before reaching its target, a ray crosses the ambient air, where no absorption loss occurs. Because the surface is defined by a repartition of height on a regular array, it was easy to determine triangular microfacets where a normal was also straightforwardly defined. When a ray hit a microfacet, its new direction

Downloaded from https://www.cambridge.org/core. University of Basel Library, on 11 Jun 2017 at 14:25:10, subject to the Cambridge Core terms of use, available at https://www.cambridge.org/core/terms. https://doi.org/10.1557/JMR.2010.0244

was then calculated using both knowledge of the surface normal and the application of Snell's laws. From an optical viewpoint, a domain defined by a microfacet was found to be opaque and its intrinsic optical properties were defined by its complex optical indexes, $\tilde{n}(\sigma, T)$. These indexes $\tilde{n}(\sigma, T)$ take into account the structural bidimensionality of the single crystal of $Pr_2NiO_{4+\delta}$ (22). Here, $\tilde{n}(\sigma, T)$ is equal to $n(\sigma, T) + i\ k(\sigma, T)$, where $n(\sigma, T)$ is the refractive index and $k(\sigma, T)$ is the extinction index.[19] These optical functions were known for a range of temperature from 300 to 1300 K.[10,20] For the $Pr_2NiO_{4+\delta}$ single crystal, the thermo-optical properties are governed by optical mechanisms linked to the charge carriers created to compensate for the presence of extra oxygen, δ. Extra oxygen leads to the injection of charge carriers that are massively injected within the *ab*-plane of the single crystal, making the physical properties of this system highly anisotropic. Thus, the *ab*-plane is often called the conducting plane, which generate an absorption coefficient, K_{ab}, with a mean value of 30,000 cm^{-1} for the spectral range spanning from far infrared up to the visible. We call to mind that $K = 4\pi k\sigma$. For the *c* axis, K_c, creates an optical contribution similar to that of a dielectric compound. Thus, the absorption coefficient of a ceramic composed of grains of $Pr_2NiO_{4+\delta}$ that are randomly oriented is around $2/3K_{ab}$ (see Fig. 4 for $T = 1000$ K). It can be concluded that a microfacet is opaque because the microfacets cover a volumetric domain with $2/3K_{ab}$ and with a mean thickness equal to 20 μm. At each striking point, an exhaust ray carried an intensity, I_{i+1} defined by

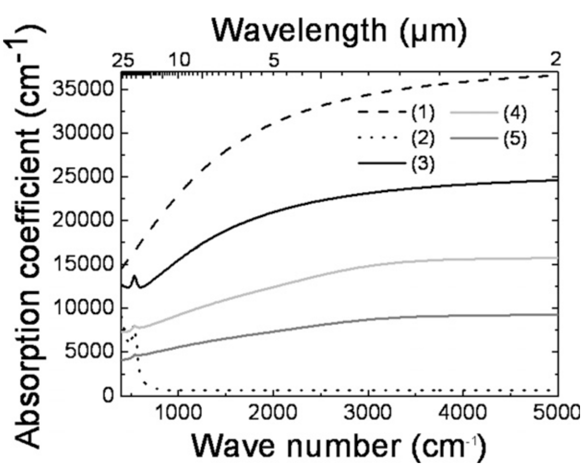

FIG. 4. Spectral dependence of the absorption coefficient of the $Pr_2NiO_{4+\delta}$ single crystal at $T = 1000$ K within the *ab*-plane (1) and along *c* axis (2). The solid line (3) corresponds to the absorption coefficient of a ceramic composed of single domain grains randomly oriented. In this case, $K_{ceramic} = 2/3K_{ab} + 1/3K_c$. Curves (4) and (5) correspond to the same ceramic but with porosities of 0.4 and 0.6, respectively.

$$I_{i+1} = \rho_i(\sigma, \theta_i, T)I_i \quad , \tag{5}$$

where $\rho_i(\sigma, \theta_i, T)$ is the local spectral directional reflectivity defined at the incidence angle θ_i. According to Fresnel's law, $\rho_i(\sigma, \theta_i, T)$ is a function of $\tilde{n}_{Pr_2NiO_{4+\delta}}(\sigma, T)$ defined in Refs. 10 and 20. Such a local process was repeated until the intensity of the ray reached a value I_{min}, after which the ray is considered to be absorbed ($I_{min} = 0$). Another way to break this recursive process is for the ray to leave the surface. Following this local process, another ray is launched. The program then counts the rays that are scattered in the upward hemisphere, $N_{scattered\ rays}$, and absorbed, $N_{absorbed\ rays}$, in the solid phase material. Finally, the hemispherical spectral reflectivity is the ratio of the number of scattered rays to the total number of rays, i.e., for a given wave number and for a given temperature

$$\widehat{R} = N_{scattered\ rays}/N_{rays} \quad .$$

When executing the MCRT code, $N_{rays} = 10^5$ were launched, which is a sensible compromise between statistical stability and computational cost. In several simulations, we checked that 10^5 rays yield statistical fluctuations smaller than 0.5%. A maximum time of 150 s is required to get a given wave number, using a single central processing unit (1.5 GHz Pentium 4). In the following, because the three surfaces characterized by SRXTM are rather similar, the one obtained at $T = 900$ K was used as the input data. For the optical functions of $Pr_2NiO_{4+\delta}$, the data previously reported at $T = 1000$ K was used (see Ref. 10 for the calculation of the optical functions). In this work, the surface measured at $T = 900$ K is supposed to be the same as the one operating at $T = 1000$ K. It is a reasonable assumption, from a material viewpoint, that no undesirable chemical evolutions can occur for the coating as well as for the ceramic substrate. As demonstrated in Ref. 4, the very slight evolution of δ in this range means that the optical functions of $Pr_2NiO_{4+\delta}$ remain the same. In fact, previous work has shown that the optical properties of $Pr_2NiO_{4+\delta}$, under air, can only change dramatically for temperatures higher than 1600 K.[21] Furthermore, prejudicial chemical reactions between the coating and the aluminosilicate substrate can occur only for temperatures around 1500 K. Moreover, no mechanical deformation is expected in the range of 900 to 1000 K, and therefore, the mechanical stability of the studied surface was rather similar at $T = 900$ K and $T = 1000$ K. From these considerations, the injection into the MCRT code of the numerical surface measured at $T = 900$ K and the optical functions of $Pr_2NiO_{4+\delta}$ calculated at $T = 1000$ K are appropriate for modeling the radiative properties of the coating at $T = 1000$ K.

Figure 5 shows a comparison between the normal spectral emissivity calculated with the SRXTM image acquired at $T = 900$ K and the one obtained through a

Downloaded from https://www.cambridge.org/core. University of Basel Library, on 11 Jul 2017 at 14:17:01, subject to the Cambridge Core terms of use, available at https://www.cambridge.org/core/terms. https://doi.org/10.1557/JMR.2010.0244

mechanical profilometer (MP) at $T = 300$ K (see Ref. 10). Results show that the spectrum calculated from the SRXTM experiment is slightly higher than the one obtained through the MP on the entire investigated spectral range. This finding can be explained by the higher spatial resolution of SRXTM (0.7 versus 1 μm for MP). However, care must be taken because the different treatments applied in this work for extracting the SRXTM image could slightly modify the geometrical description of the real surface. Figure 6 indicates that the average number of scattering events before absorption is more important for the SRXTM image than for the MP image. Once again, the procedure used for the reconstruction of the SRXTM can generate more pronounced slopes, α, that increase the normal spectral emissivity. Even if the surface is not perfectly Gaussian, the comparison of the α_{SRXTM} and α_{MP} can be used qualitatively as a useful guideline. One recalls that for a Gaussian surface:

$$\alpha = \sqrt{2}\frac{\omega_{rms}}{\tau} \quad , \tag{6}$$

and from Table I, $\alpha_{SRXTM} > \alpha_{MP}$. In fact, it is well known that for an opaque rough surface, the normal spectral emissivity is higher for higher α.[2] Moreover, recent works of Bergstrom and coworkers[2] demonstrated that for normal incidence, according to the value of $\alpha/\sqrt{2}$, different regions can be distinguished to explain the increase in the normal spectral emissivity of a rough opaque system. In particular, our findings are consistent with the results calculated by Bergrstrom and coworkers for the region where

$$0.15 < \alpha/\sqrt{2} < 2 \quad .$$

Bergstrom and coworkers found that the threshold for double scattering is around $\omega_{rms}/\tau \sim 0.15$, as reported in Fig. 5 of this work. Nevertheless, for the MP image, the use of the region proposed by Bergtrsom and coworkers does not match our findings. High-temperature SRXTM can also provide suitable 3D images to perform MCRT simulations. However, this section highlights that the spatial resolution of this technique, which probes the surface, implies the use of mathematical operations to treat the image. In turn, the mathematical operations affect the final result. Figure 7 makes a comparison between the numerical spectral emissivity obtained from the SRXTM image and the one obtained experimentally at $T = 1000$ K on the same ceramic.[12] The normal spectral emissivity of a fictitious ceramic of $Pr_2NiO_{4+\delta}$ with a thickness of 20 μm is also reported. As previously stated, the fictitious ceramic is made of randomly oriented single crystalline grains. The emissivity of the ceramic is increased by a factor 1.2 on the whole spectrum when the ceramic becomes rough. Nevertheless, a gap between simulated and experimental values suggests that the optical contribution due to surface roughness cannot be explained exclusively by the high normal spectral emissivity of the coating of $Pr_2NiO_{4+\delta}$. An investigation of the morphology of the grains by ESEM indicates that they show a microscale roughness at their surfaces and

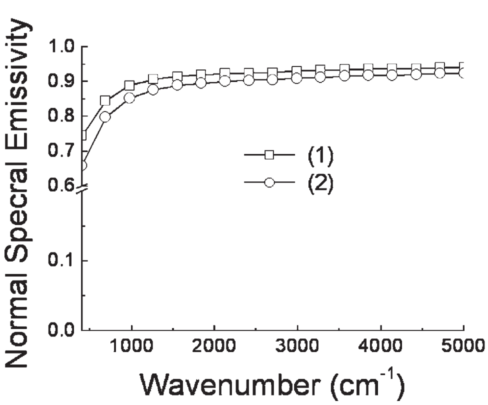

FIG. 5. Calculated normal emissivity spectra at $T = 1000$ K from (1) a reconstructed image obtained at $T = 900$ K by SRXTM and (2) a reconstructed image obtained at $T = 300$ K by mechanical profilometry. Note that for SRXTM, the pixel size was 0.7 μm and for MP, it was 1 μm.

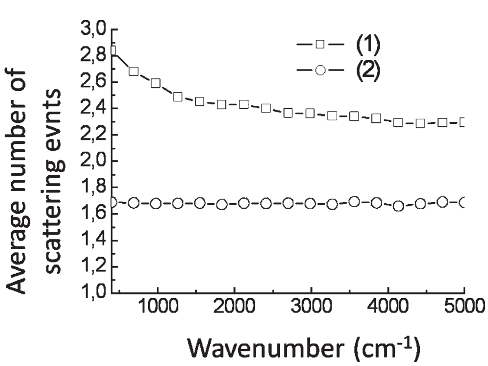

FIG. 6. Average number of scattering events reported when the SRXTM image (1) is used and when the PM image (2) is used.

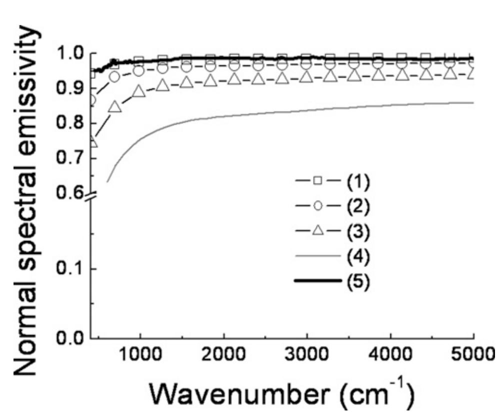

FIG. 7. Normal spectral emissivity of the numerical rough ceramic of $Pr_2NiO_{4+\delta}$ at $T = 1000$ K with a volume fraction of heterogeneity of (1) 0.6, (2) 0.4, (3) 0.0. Curve (4) corresponds to the normal spectral emissivity of the flat $Pr_2NiO_{4+\delta}$ ceramic and curve (5) to the one experimentally measured by infrared emission spectroscopy (see Ref. 12).

Downloaded from https://www.cambridge.org/core. University of Basel Library, on 11 Jul 2017 at 14:25:10, subject to the Cambridge Core terms of use, available at https://www.cambridge.org/core/terms. https://doi.org/10.1557/JMR.2010.0244

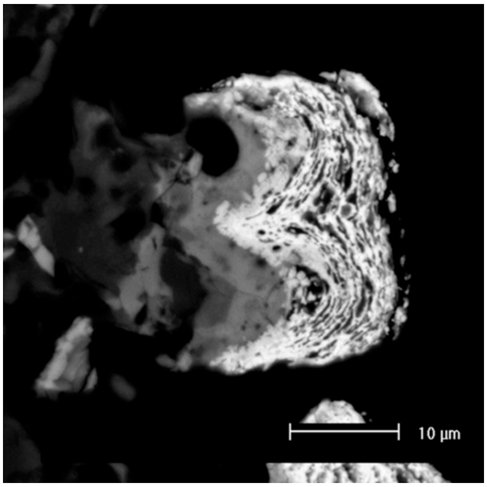

FIG. 8. ESEM image of the interior of a grain (2000×).

pores with submicron size in their own volume, as can be seen in Fig. 8. The typical mean size is around 300 nm. Such an observation suggests that a second optical contribution due to the texture of the coating can be added to model its global optical response. Taking into account the submicron contribution, the effective medium approximation (EMA) can be used. Indeed, when the length scale of heterogeneity is much smaller than the incident wavelength, the use of the EMA enables one to consider that radiation propagates within the heterogeneous medium as if it were homogeneous.[22–24] Hence, the propagation of radiation can be studied in a much simpler way by introducing homogeneous equivalent optical functions. Many approaches have been proposed to model this phenomenon and have been extensively studied in the literature.[22,24] For this work, the Bruggeman model is used. It allows for the modeling of polydispersed spheres filled with air homogenously distributed in a continuous medium. Another benefit of this model is to follow the evolution of the optical functions on a large domain of volume fraction, p, with $0 < p < 1$. In this work, one assumes that both of the heterogeneities (internal porosity and external microroughness) satisfied Bruggeman's law. More details concerning the influence of p on the optical function can be found in Ref. 10.

As shown in Fig. 4, the effective absorption coefficient of the ceramic of $Pr_2NiO_{4+\delta}$ is lower for a higher p value. As a direct consequence, the penetration depth of the infrared light increases from 2.5 μm for $p = 0$ up to 11 μm for $p = 0.7$. In other words, the MCRT code can use effective optical functions that take into account the submicron heterogeneity of the coating with a thickness of 20 μm. In Fig. 7, two curves that were calculated by combining the MCRT code with the optical function of the EMA to the SRXTM image are plotted. The best results are obtained with $p = 0.6$. This value appears rather high because the analysis of the ESEM images of a collection of grains suggests that the internal porosity is around 0.4.[10] Moreover, the proportion of submicron roughness on a grain is difficult to estimate. Furthermore, a higher magnification of the SRXTM image (Fig. 9) suggests that several shadowed regions are not integrated into the modeling of the optical response.[2] Minimally, it shows that a multiscale study of both the texture and chemical composition of a black body coating can reproduce its optical response. The combination of MCRT and EMA brings possibilities to deal with porous opaque mediums for which sizes of heterogeneities are typically distributed on two different length scales: submillimeter and submicron. Furthermore, in the case of a rough opaque ceramic with submicron heterogeneities, the normal spectral emissivity straightforwardly depends on $\tilde{n}(\sigma, T)$, $\omega_{rms}(T)$, $\tau(T)$, and $p(T)$. Such a relation can be used, in return, to design opaque materials with the desired normal spectral emissivity.

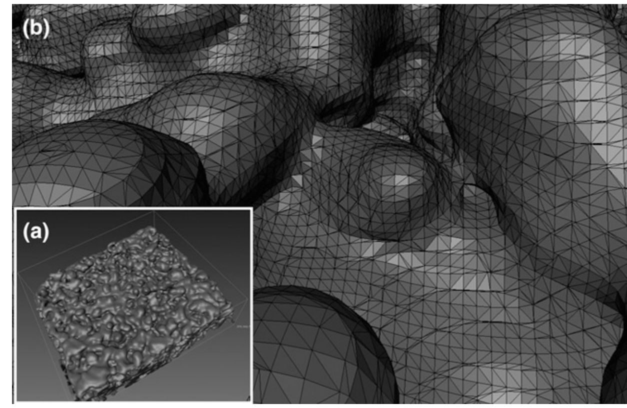

FIG. 9. View of the SRXTM image of the rough surface with two magnifications: (a) low magnification and (b) high magnification.

IV. CONCLUSION

In this work, high temperature SRXTM has been used to characterize the surface geometry of a $Pr_2NiO_{4+\delta}$ ceramic on a range of temperatures from 300 to 900 K. The experiments combine the setup available at the TOMCAT beamline of SLS and a monitored gas blower furnace that allows heating of the ceramic in air. Specific image treatment allows for the extraction of the rough surfaces. Statistical characterization of a set of surfaces indicates that the geometry is not altered by heating and that a MCRT code can be useful to model their optical responses at $T = 1000$ K. For this purpose, the optical functions of $Pr_2NiO_{4+\delta}$, calculated at $T = 1000$ K, and the surface, measured at $T = 900$ K, are used as input data. The surface measured at $T = 900$ K is assumed to have the same morphological features as the one operating at $T = 1000$ K. However, the MCRT code, applied to

Downloaded from https://www.cambridge.org/core. University of Basel Library, on 11 Jul 2017 at 21:54:17, subject to the Cambridge Core terms of use, available at https://www.cambridge.org/core/terms. https://doi.org/10.1557/JMR.2010.0244

the hottest surface, cannot provide a satisfactory result because of a gap between the reconstructed normal emissivity spectrum and the experimental one. The combination of the MCRT code with EMA allows for good agreement between the modeling and the measurement. This work shows that a multiscale approach is necessary to understand and predict the behavior of such black oxide ceramics. In particular, the normal spectral emissivity is, in this case, a function of the chemical composition and the texture, which are both integrated into the model by injecting the complex optical index of the solid phase, $\tilde{n}(\sigma, T)$, the rms of the height, $\omega_{\rm rms}^2$, the correlation length, τ, and the volume fraction of the submicron heterogeneities, p. This study demonstrates a new method for designing opaque materials with a specific normal spectral emissivity.

ACKNOWLEDGMENTS

This work was supported by the French National Research Agency (ANR JCJC-0028). The authors thank E. Veron (CEMHTI) for ESEM measurement. They acknowledge E. Boller (ESRF, Grenoble, France) for helpful advice and P. Van der Linden, B. Gorges, and H. Vitoux for the loan of the gas blower furnace. The authors also thank Dr. F. Marone and G. Mikuljan (SLS, Villingen, Switzerland) for helpful assistance during the experiments at SLS. D. De Sousa Meneses and P. Echegut (CEMHTI, Orleans, France) are also acknowledged for discussions concerning the implementation of the MCRT code. Finally, the authors acknowledge J. Baruchel (ESRF, Grenoble, France) for motivating recommendations. The authors wish to thank D. Asselot and P. Estrade (VSG, Mérignac) for helpful discussions concerning the use of Avizo. The help of M. Brinas has been appreciated for having read grammar and spelling.

REFERENCES

1. K. Tang and R.O. Buckius: A statistical model of wave scattering from random rough surfaces. *Int. J. Heat Mass Transfer* **44,** 2001 (2001).
2. D. Bergstrom, J. Powell, and F.H. Kaplan: The absorption of light by rough metal surfaces—A three-dimensional ray-tracing analysis. *J. Appl. Phys.* **103,** 103515 (2008).
3. H. Gomart: Modeling of thermal radiative properties of high emissive coatings. Ph.D. Thesis, University of Orléans, France, 2008.
4. M. Van Geet and R. Swennen: Quantitative 3D-fracture analysis by means of microfocus x-ray computer tomography (μCT): An example from coal. *Geophys. Res. Lett.* **28,** 3333 (2001).
5. P. Gouze, C. Noiriel, C. Bruderer, D. Loggia, and R. Leprovost: X-ray tomography characterization of fracture surfaces during dissolution. *Geophys. Res. Lett.* **30,** 1267 (2003).
6. H. Proudhon, J-Y. Buffière, and S. Fouvry: Characterisation of fretting fatigue damage using synchrotron x-ray micro-tomography. *Tribol. Int.* **39,** 1106 (2006).
7. C. Laforsch, E. Christoph, C. Glaser, M. Naumann, C. Wild, and W. Niggl: A precise and non-destructive method to calculate the surface area in living scleractinian corals using x-ray computed tomography and 3D modeling. *Coral Reefs* **27,** 811 (2008).
8. ESRF: http://www.esrf.eu/UsersAndScience/Experiments/Imaging/ID19/. Accessed October 1, 2009.
9. J.A. Ogivily: *Theory of Wave Scattering from Random Rough Surfaces*, 1st ed. (Taylor and Francis, Bristol, 1991), p. 292.
10. H. Gomart, B. Rousseau, D. De Sousa Meneses, and P. Echegut: Multiscale approach for predicting the radiative behavior of opaque ceramics with micro and macro scale heterogeneities. *J. Appl. Phys.* (Submitted).
11. B. Rousseau, H. Gomart, D. De Sousa Meneses, P. Echegut, M. Rieu, R. Dugas, P. Lenormand, and F. Ansart: Modelling of the radiative properties of a porous ceramic layer. *J. Electr. Ceram.* (accepted), DOI: 10.1007/s10832-009-9595-6.
12. B. Rousseau, A. Sin, P. Odier, F. Weiss, and P. Echegut: High emissivity of a rough Pr_2NiO_4 coating. *Appl. Phys. Lett.* **79,** 3633 (2001).
13. M. Stampanoni, A. Groso, A. Isenegger, G. Mikuljan, Q. Chen, A. Bertrand, S. Henein, R. Betemps, U. Frommherz, P. Böhler, D. Meister, M. Lange, and R. Abela: Developments in x-ray tomography, in *Proc. SPIE*, Vol. 6318, edited by U. Bonse (San Diego, CA, August 13–17, 2006), pp. 63180M1-14.
14. ESRF: Hot air blower. http://www.esrf.eu/UsersAndScience/Experiments/TBS/SampleEnvironment.
15. NIST: X-ray form factor, attenuation, and scattering tables. http://physics.nist.gov/PhysRefData/FFast/html/form.html. Accessed October 1, 2009.
16. K. Fu and P.F. Hsu: New regime map of the geometric optics approximation for scattering from random rough surfaces. *J. Quant. Spectrosc. Radiat. Transfer* **109,** 180 (2008).
17. H.J. Lee, Y.B. Chen, and Z.M. Zhang: Directional radiative properties of anisotropic rough silicon and gold surfaces. *Int. J. Heat Mass Transfer* **49,** 4482 (2006).
18. B. Rousseau, D. De Sousa Meneses, P. Echegut, M. Di Michiel, and J.F. Thovert: Prediction of the thermal radiative properties of an x-ray-tomographied porous silica glass. *Appl. Opt.* **46,** 4266 (2007).
19. M. Born and E. Wolf: *Principle of Optics, Electromagnetic, Theory of Propagation, Interference and Diffraction Light*, 7th ed. (Cambridge Univ. Press, Cambridge, 1999), pp. 1–70.
20. B. Rousseau, D. De Sousa Meneses, A. Blin, P. Echegut, M. Chabin, P. Odier, and F. Gervais: High-temperature behavior of infrared conductivity of a $Pr_2NiO_{4+\delta}$ single crystal. *Phys. Rev. B* **72,** 104114 (2005).
21. B. Rousseau, J.F. Brun, D. De Sousa Meneses, and P. Echegut: Temperature measurement: Christiansen wavelength and blackbody reference. *Int. J. Thermophys.* **26,** 1277 (2005).
22. D.E. Aspnes, J.B. Theeten, and F. Hottier: Investigation of effective-medium models of microscopic surface roughness by spectroscopic ellipsometry. *Phys. Rev. B* **20,** 3292 (1979).
23. B. Rousseau, A. Canizares, E. Véron, R. Ramy-Ratiarison, A. Blin, D. De Sousa Meneses, P. Simon, F. Berberich, H. Graafsma, A. Pomar, N. Mestres, T. Puig, and X. Obradors: Characterization of $YBa_2Cu_3O_{6+x}$ films grown by the trifluoroacetate metal organic decomposition route by infrared spectroscopy. *Thin Solid Films* **515**(4), 1607 (2006).
24. M.M. Braun and L. Pilon: Effective optical properties of non-absorbing nanoporous thin films. *Thin Solid Films* **496,** 505 (2006).

Downloaded from https:/www.cambridge.org/core. University of Basel Library, on 11 Jul 2017 at 14:27:10, subject to the Cambridge Core terms of use, available at https:/www.cambridge.org/core/terms. https://doi.org/10.1557/JMR.2010.0244